PRAMANA — journal of physics

Vol. 84, No. 6
June 2015
pp. 1087–1098

Colloidal transparent conducting oxide nanocrystals: A new infrared plasmonic material

BHARAT TANDON, ASWATHI ASHOK and ANGSHUMAN NAG*
Department of Chemistry, Indian Institute of Science Education and Research (IISER), Pune 411 008, India
*Corresponding author. E-mail: angshuman@iiserpune.ac.in

DOI: 10.1007/s12043-015-1008-6; ***e*Publication:** 2 June 2015

Abstract. Thin films of transparent conducting oxides (TCO) are technologically important for applications as a visible light transparent electrode in a wide variety of optoelectronic devices. In the last few years, researchers started to explore novel size- and shape-dependent properties of TCO, where the crystallite size is ∼10 nm. So far, the localized surface plasmon resonance (LSPR) properties of TCO nanocrystals (NCs) have been found to be the most interesting. TCOs like Sn-doped In_2O_3, Al-doped ZnO and In-doped CdO NCs, exhibit LSPR band in near- to mid-infrared region. LSPR from a TCO NC exhibits many intrinsic differences with that of a metal NC. Carrier density in a TCO NC can easily be tuned by controlling the dopant concentration, which allows the LSPR band to be tuned over a range of ∼2000 nm (∼0.62 eV) in the near- to mid-infrared region. This review discusses recent advances in the understanding of plasmonic properties of various TCO NCs and highlights the potential applications of such unique plasmonic properties.

Keywords. Near-infrared plasmonics; transparent conducting oxide nanocrystals; doped semiconductor nanocrystals.

PACS Nos 81.07.Bc; 78.67.Bf; 73.20.Mf

1. Introduction

Transparent conducting oxides (TCOs) are materials that combine the normally mutually exclusive properties of electrical conductivity and visible light transparency [1,2]. Combination of both properties make TCOs indispensable in the optoelectronic industry as transparent electrodes for solar cells, light emitting diodes and flat panel displays. The global market for such transparent coatings was $4.8 billion in 2013 and is expected to increase rapidly to $7.1 billion by 2018 [3]. Clearly, TCOs are popular as transparent conductors. However, in this review, we shall discuss about a new property, namely, plasmonics of TCOs, which arises when the crystallite size becomes a few nanometres.

Localized surface plasmon resonance (LSPR) from different metal nanocrystals (NCs) has been studied in depth for more than two decades now [4–6]. More recently, LSPR has also been obtained from doped semiconductor NCs. For example, both Sn-doped In_2O_3 (ITO) [7] and non-stoichiometric $Cu_{2-x}S$ NCs [8] show strong LSPR bands. In all the cases, LSPR band arises from free charge carriers. If heavy doping (or vacancies) can provide enough free electrons (holes) in conduction (valance) band of the host, then LSPR appears. Bulk TCOs, such as ITO, exhibit metallic charge transport because of high concentration of free electrons in the conduction band. This aspect of TCOs has encouraged researchers to prepare tiny NCs of TCOs, such that the high free electron density can give rise to LSPR. Expectedly, LSPR obtained from such TCO NCs exhibits many intrinsic differences with that of metal NCs.

Schematic inserted in figure 1a shows free electron oscillation from a TCO NC, which is similar to that of a metal NC. However, the LSPR from TCO exhibits the following features which are distinctly different from that of metal NCs: (i) Free electron density can be tuned by tuning the dopant concentration in TCO which gives a LSPR band tunable from near-infrared (NIR) to mid-IR (∼1300 to 4000 nm) range but such tuning of carrier density is not possible for metal NCs [9]. (ii) Excited states of TCO NCs have both bound excitons and free electrons, which is not the case for metal NCs. For example, figure 1a shows that the undoped In_2O_3 NCs exhibit sharp excitonic feature at around 4.1 eV. However, after doping with Sn^{4+}, 10% Sn-doped In_2O_3 NCs do not show excitonic feature because the free electrons generated after Sn doping screen the Coulomb interaction between the bound electron–hole pair (exciton) [10]. There are scopes to explore interactions between free electrons and weak transient excitons in TCO NCs. (iii) TCO can be codoped also, such as in Fe–Sn codoped In_2O_3 NCs, where free electrons from Sn^{4+} interacts with magnetic spins from Fe^{3+}, manifesting interesting magnetoelectric and magneto-optic properties, but such interactions are not possible in metal NCs [11].

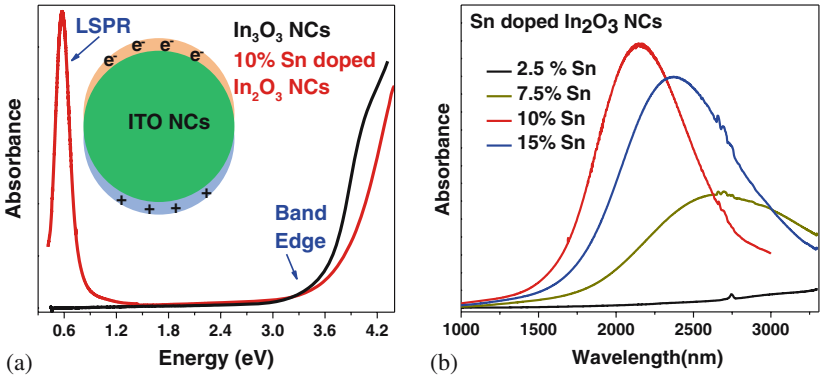

Figure 1. (**a**) Comparison of UV−visible−NIR absorption spectra of 10% Sn-doped and undoped In_2O_3 NCs showing LSPR band in the NIR region and increase in band gap along with bleaching of exciton feature in the UV region for doped NCs. Schematic shows free carrier oscillation responsible for LSPR band in 10% Sn-doped In_2O_3 (ITO) NCs. (**b**) UV−visible−NIR absorption spectra of Sn-doped In_2O_3 NCs showing the effect of dopant concentration on the LSPR band (reprinted with permission from ref. [10]).

(iv) TCO NCs are visible light-transparent, whereas metal NCs typically show strong LSPR band in the visible region. The NIR and mid-IR LSPR from TCO NCs can complement visible LSPR from metal NCs for applications in different spectral ranges.

There are three recent reviews on LSPR from doped semiconductor NCs [12–14]. The present review mainly highlights unique features of LSPR from TCO NCs and their applications, which were not discussed in previous review articles. This review will further be divided into three subsections: (a) correlation between free electron density and LSPR band in ITO NCs, (b) various TCO NCs exhibiting LSPR band and (c) applications.

2. Correlation between free electron density and LSPR band in ITO NCs

ITO being one of the most famous TCO in bulk and thin film, has also found dominance in NC research among other TCO NCs. Origin of LSPR band has been investigated in more detail for ITO NCs compared to other TCO NCs.

2.1 *Drude model and LSPR band*

The basic assumption of classical Drude model includes a metal to be formed completely of ions from which some electrons have been detached. These electrons behave as a 'free electron gas' and being an ideal gas are completely free of any long-range electron–electron or electron–ion interaction. The various electrical and thermal properties of a metal are attributed as a direct consequence of the collective behaviour of these free electrons [15]. The collective oscillations of these so-called 'free electrons' upon irradiation of an electromagnetic radiation of suitable frequency give rise to a LSPR band. LSPR frequency depends by a small factor on shape, size and local medium and is primarily governed by change in carrier density of the material [16,17]. LSPR frequency increases with increasing carrier density. Using classical Drude model, LSPR frequency is determined by the relation:

$$\omega_{\mathrm{sp}} = \sqrt{\frac{N_{\mathrm{c}} e^2}{(\varepsilon_\infty + \varepsilon_{\mathrm{m}})\, \varepsilon_0 m_{\mathrm{c}}} - \gamma^2}, \tag{1}$$

where ω_{sp} is the LSPR frequency, N_{c} is the free carrier density, e represents the electronic charge, ε_0 is the absolute permittivity of air/vacuum, ε_{m} is the dielectric constant of the medium, ε_∞ is the dielectric constant at high frequency when all the polarization mechanisms die out, m_{c} is the effective mass of the carrier and γ is the bulk collision frequency which can also be determined by measuring the linewidth in the LSPR spectrum [18]. This relation ignores any contribution from interband transitions. However, if there is any overlap between the interband transition and LSPR energy, coupling is expected between the two transitions and dielectric response is affected in that case which is taken care of by adding an extra term to the expression.

Metal NCs like Ag and Au having high free electron densities (10^{22}–10^{23} cm^{-3}) exhibit LSPR in the visible region [17], but degenerately-doped semiconductor NCs with lower free electron densities (10^{20}–10^{21} cm^{-3}) exhibit LSPR in NIR to mid-IR region [19]. The tail of NIR LSPR from doped semiconductor NCs also extends to the red region of the electromagnetic spectrum. Therefore, TCO NCs exhibit the complementary blue

colour. Though Drude model was originally formulated for metals [18], its application was extended to doped semiconductor nanocrystals as well. Though it can explain the free charge carrier densities in the case of larger NCs (where size is much greater than the De Broglie wavelength of the carrier), it cannot quite explain the behaviour of the smaller NCs quantitatively, particularly due to two reasons; (i) scattering of charge carriers by the nanocrystal surface and (ii) carrier localization in the case of NCs having diameters less than the Bohr-exciton radius as reported by Gamelin *et al* [20]. The deviation from Drude model was attributed to the presence of quantum plasmons that were partially localized [21] and quantitative description of semiconductor NCs thus requires the inclusion of quantum mechanical treatment too which was provided by the Lorentz oscillator model [20].

If the resistivity (ρ) of the material is known, then the carrier density obtained by Drude model can also be used to calculate the mobility (μ) of carriers using eq. (2) [22].

$$\mu = \frac{1}{N\rho e}. \tag{2}$$

Figure 1b shows the NIR absorption spectra of Sn-doped In_2O_3 NCs with varying Sn content and exhibiting cubic bixbyite structure. The LSPR resonance wavelength shifts to lower values with an increase in absorbance as the Sn concentration increases from 2.5 to 10%, because of the increase in free electron concentration with doping concentration as predicted by the Drude model. However, further increase in dopant concentration up to 15%, shifts the LSPR band towards longer wavelengths because of the electron trapping by the dopant ions [19] discussed in the following subsection.

2.2 *Mechanism of generation of free electrons in ITO NCs*

Transmission electron microscopy (TEM) image in figure 2a shows the size of ITO NCs is 6.5 nm. Figure 2b shows NIR absorption spectrum of 10% Sn-doped In_2O_3 NCs at different reaction times. It is observed that the LSPR band appears only after the reaction has proceeded for 60 min in an inert atmosphere as shown in figure 2b. As the reaction time increases, both the LSPR peak absorbance and peak energy increases (wavelength decreases). As mentioned earlier, intensity and position of a LSPR peak depend upon the shape, size, dielectric constant of a medium and number of free charge carriers. One might speculate about which of these factors is affecting the position of LSPR. TEM results show similar size of NCs after 60 min and 3 h of reaction but with a very different LSPR band. Also, doping in small concentrations does not change the dielectric constant of the local medium by a significant amount. Therefore, the change in LSPR with reaction time is due to the change in electron density, which depends upon doping of Sn^{4+} ions. However, elemental analysis (EDAX and ICP-OES) showed similar Sn content for both NCs obtained after 60 min and 3 h of reaction time. It is to be noted that such elemental analysis cannot distinguish between Sn on the surface and in lattice of the NC, but the spectral width of LSPR band can suggest about the location of dopant ions. It was recently shown that LSPR spectrum is narrower when Sn^{4+} is on the surface of In_2O_3 NC, compared to Sn^{4+} doped into the core lattice [23]. Figure 2b (also when x-axis is plotted in the unit eV) does not show any broadening of LSPR bandwith reaction time and therefore the possibility of slow diffusion of dopant ions from the surface to the core of

NC with reaction time, thereby, exhibiting LSPR at a longer reaction time can be ignored. Then, the reasons for a slow release of free electrons with reaction time, thus exhibiting LSPR band after a longer reaction time, need to be found.

In bulk Sn-doped In_2O_3, one oxygen vacancy leads to the generation of two electrons following the equation given by De Wit [24–27]

$$O_O^x \leftrightarrow 2e' + V_O^{\cdot\cdot} + \frac{1}{2}O_2, \tag{3}$$

where the subscript refers to the site name, superscript refers to the charge on the defect site (x for neutral, ($'$) refers to a negative charge on the defect site and ($^{\cdot}$) refers to a positive charge on the defect) according to Kröger–Vink notation [28]. For example, O_O^x refers to an oxygen atom present on an oxygen site with a neutral charge on the defect site.

On the other hand, according to Frank and Köstlin model for ITO [29], at low doping levels, each Sn^{4+} contributes an e^- to the conduction band of In_2O_3 following eq. (4)

$$(O_i''2Sn_{In}^{\cdot})^x \leftrightarrow 2Sn_{In}^{\cdot} + 2e' + \frac{1}{2}O_2, \tag{4}$$

where $Sn_{In}^{\cdot}$ represents a Sn^{4+} substituting a In^{3+} site leaving a positive charge on the defect site and O_i'' represents an oxygen atom present at an interstitial position leaving a -2 charge at the defect site. Each interstitial oxygen is found to be associated with two Sn^{4+} ions forming a reducible cluster giving two e^- on reduction following eq. (4). At higher levels of doping, formation of irreducible clusters and aggregated clusters having three or four Sn associated with each interstitial oxygen has been formulated. These aggregated/non-reducible clusters reduce the effective free carrier concentration per Sn dopant [29,30].

Is it the same reaction represented by eq. (4) which is responsible for a slow release of free electron in ITO NCs and therefore exhibiting LSPR band at a longer a reaction time? To verify this aspect, ITO NCs were prepared at different oxygen partial pressures and the corresponding LSPR behaviour is shown in figure 2c. When the reaction was carried out in air, no LSPR peak was observed even after 3 h of the reaction. LSPR peak appeared after 60 min of the reaction when carried out in nitrogen, and the LSPR peak appeared just after 45 min of the reaction when the reaction was carried under a reducing gas mixture (90% N_2+ 10% H_2). The colour (inset to figure 2b) of the NC solution after 3 h was blue for NCs prepared under N_2 or under the reducing gas mixture because the tail of NIR LSPR absorption is extended up to the red region, whereas, the NCs remained colourless (inset to figure 2b) when the reaction was carried for 15 min under N_2. We note here that the blue colour signifying the NIR LSPR band is absent for NCs when the reaction was carried out in air even after 3 h. All other characterizations such as size of the NC, dopant concentration and crystal structure of ITO NCs remained unaltered for all three reaction environments, namely air, N_2 and reducing gas mixture. Therefore, the drastic change in LSPR behaviour observed for reactions carried out under different oxygen partial pressure can be explained by eq. (4). Lowering oxygen partial pressure shifts the equilibrium of the reaction towards the right-hand side, therefore releasing free electrons exhibiting LSPR band. Thus, the slow release of electrons in ITO NCs is attributed to slow reduction of the

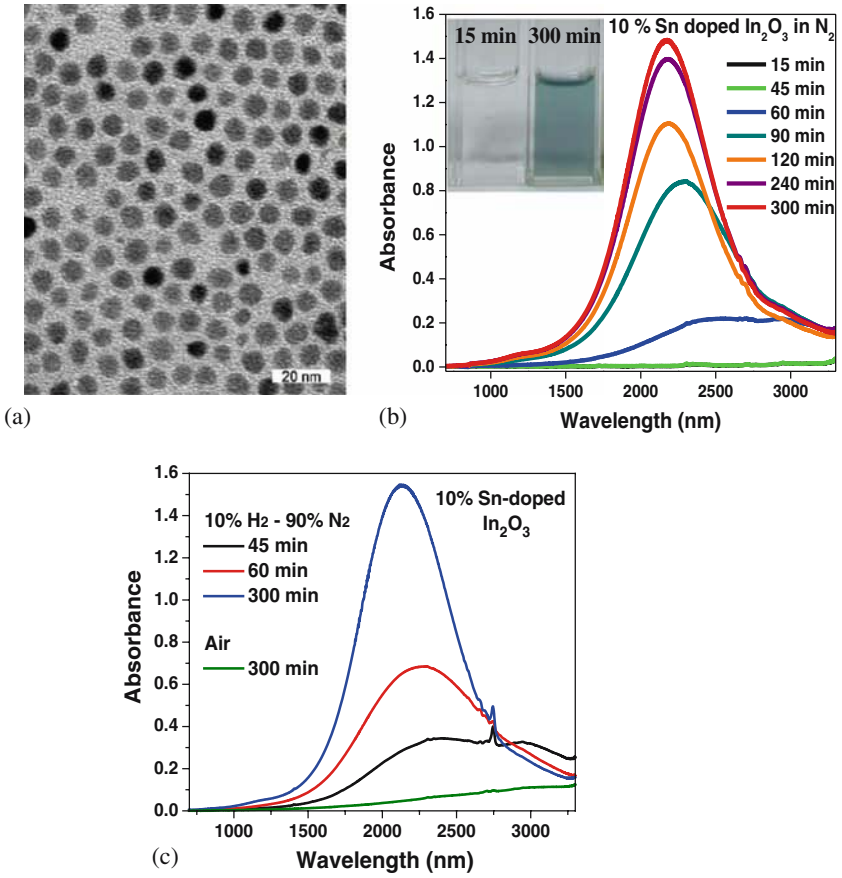

Figure 2. (**a**) TEM image of 10% Sn-doped In_2O_3 NCs after 60 min of reaction in N_2 environment. (**b**) Absorption spectrum showing the growth of LSPR band at different time intervals for a reaction carried under N_2 environment. Inset shows photographs of 10% Sn-doped In_2O_3 NCs dispersed in tetrachloroethylene at 15 min and 300 min respectively. (**c**) Comparison of intensity of LSPR bands at different time periods in different reaction atmospheres, namely, air and 10% H_2–90% N_2 mixture (reprinted with permission from ref. [11]).

reducible $(O_i''2Sn_{In}^{\cdot})^x$ cluster which in the case of bulk ITO also takes a long time even at elevated temperatures [29].

We note here that the density of oxygen vacancies is limited to a small concentration, and therefore, oxygen vacancies alone cannot give rise to sufficient electron density, yielding no LSPR band from undoped In_2O_3 NCs, even after preparing under a reducing environment. The choice of the dopant and the host material should be such that the dopant generates shallow electron donor states near the conduction band of the electrons. Bulk TCOs are known for having such shallow electron donor states, which is the reason behind exploring TCO NCs for LSPR.

3. Various TCO NCs exhibiting LSPR band

Other TCO NCs, apart from ITO NC, have been explored in the last two years and different major systems showing strong LSPR bands have been discussed below.

3.1 *Al-Doped ZnO NCs*

Need for the development of a cheaper and less toxic TCO material led to the synthesis of doped zinc oxides (doping with In, Al, B, F, Ga) in the bulk form or as thin films [31]. ZnO having a band-gap energy of 3.3 eV is transparent in the visible region, and n-type doping with Al, Ga and In provides excess free electron concentration in the conduction band leading to electrical conductivity. Milliron *et al* reported the synthesis of Al-doped ZnO NCs, where the free electron concentration is sufficient to exhibit strong LSPR band in mid-IR region [32]. Zinc stearate and aluminium acetylacetonate were used as the precursors along with oleic acid, octadecene and hexadecanediol to prepare Al-doped ZnO NCs. Al doping is favoured in ZnO lattice due to the similar ionic radii and electronegativities of Al^{3+} and Zn^{2+}. Jasieniak *et al* recently reported a generic synthesis of Al, Ga and In-doped ZnO NCs exhibiting NIR LSPR [33].

3.2 *In-Doped CdO NCs*

In^{3+}-doped bulk CdO is a well-studied TCO material. In^{3+} can be doped easily in CdO because of the similar ionic radii of Cd^{2+} and In^{3+}. The first synthesis of In-doped CdO NCs was reported by Murray and coworkers [34]. Morphology of the NCs was tuned by varying capping ligand concentration and reaction temperature. These In-doped CdO NCs show strong plasmonic absorption which can be tuned from 1.8 to 3.5 μm depending on the percentage of In doping. It is observed that the shape and size of the NC can influence the LSPR band (figure 3). In spherical ICO NCs, LSPR peak at 3296 nm is highly symmetrical while smaller octahedral NCs display broader peak at 3606 nm, and large octahedral NCs show two peaks at 2507 nm and 3898 nm.

3.3 *F and In-codoped CdO*

In addition to cation doping, anion doping can also increase the free electron concentration which shifts the LSPR band to higher energies [35]. Fluorine doping is done in ICO to improve the optical quality and charge-carrier mobility. Use of InF_3 as a precursor helps in simultaneous incorporation of In and F into the CdO lattice. Since F^- (1.33 Å) and O^{2-} (1.40 Å) have close ionic radii, and fluorine atom is more electronegative than the oxygen atom, fluorine incorporation into the lattice can readily occur. Sharp LSPR bands tunable between 1.5 and 3.3 μm have been displayed by F and In-codoped CdO. F and In-codoped CdO NCs exhibit the highest LSPR quality factor (12.2) reported so far among all TCO NCs. The LSPR quality factor, $Q = E/\Delta E$, is the ratio between LSPR energy (E) and full-width at half-maximum (FWHM) of the LSPR band (ΔE).

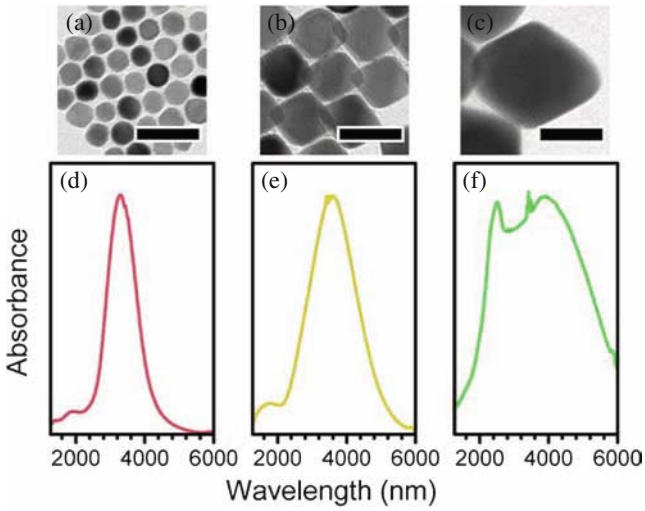

Figure 3. The TEM images of In-doped CdO NCs showing (**a**) spherical, (**b**) small octahedral and (**c**) large octahedral NCs. Scale bar = 50 nm for all images. UV−visible−NIR absorption spectra of In-doped CdO NCs for (**e**) spherical, (**f**) small octahedral and (**g**) large octahedral NCs, dispersed in CCl_4 (reprinted with permission from ref. [34]).

3.4 *Photoexcited ZnO NCs*

LSPR peaks can arise not only from equilibrium steady-state population of the doped semiconductors, but also from photoexcited undoped semiconductors [36,37]. ZnO has been used as a model system to demonstrate that non-equilibrium carrier population can also display LSPR bands. ZnO NCs absorb photon with energy higher than or equal to band gap producing bound electron–hole pair as shown schematically in figure 4, where the electron is in the conduction band and the hole is in the valence band. The hole in the valence band can be scavenged by alcohol or hydroxyl group liberating protons in solution. These excited electrons are accumulated in the conduction band in the absence of electron scavengers like oxygen and give rise to LSPR bands in the IR region.

4. Applications

Research activity in LSPR of TCO NCs has intensified in the last few years. Presently, work is mainly focussed on developing new TCO NCs and understanding their LSPR properties. LSPR from TCO has not been explored enough for different applications. Two of the several possible applications of this new variety of LSPR materials have been discussed below.

4.1 *Electrochemical modulation of LSPR band and electrochromic smart window*

Milliron *et al* [38] have demonstrated dynamic tuning of LSPR band of ITO NC films through a fully reversible electrochemical process. To achieve dynamic modulation,

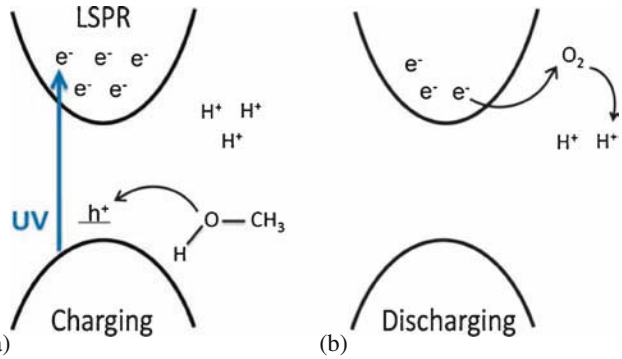

Figure 4. (**a**) Schematic representation of charging ZnO NCs (∼3 nm average diameter) after irridation with UV light having energy higher than the band gap of the NC. Methanol scavenges the hole followed by the accumulation of free electrons in the conduction band resulting in an infrared LSPR band. (**b**) Schematic representation of the discharge, when the excited ZnO NC is exposed to oxygen or electron scavengers. Direction of electron flow is indicated by curved arrows (reprinted with permission from ref. [36]).

∼150 nm thick films of ITO NCs with desired doping concentration were prepared. Bulky oleic acid capping ligands were exchanged with small-sized formic acid to improve electrical coupling between adjacent ITO NCs in the film [39,40]. The NC films were positioned as a working electrode in an electrochemical cell for active modulation of their LSPR as a function of applied voltage (figure 5a). The films showed an increase in both peak energy and absorbance, as a negative bias voltage was applied because of the increase in free carrier concentration. The potential was varied between 1.5 V and 4 V vs. the Li-based electrolyte/Li electrode system, which is the same as the potential range of -1.55–0.95 V for Ag/Ag^{+} reference electrode. The modulation of the free electron concentration and therefore the modulation of the LSPR peak was reversible and stable within the range of applied potential.

Such electrochemical modulation of NIR transmittance is vital for dynamic 'smart window' applications. Electrochromic smart window is a thin film on glass, which changes transmittance of solar spectrum, in response to an applied electric field [41]. Such smart windows help to maintain room temperature (either by heating or cooling) inside a highly glazed building through modulating the transmittance of sunlight. Figure 5b shows transmittance of solar spectrum in AM 1.5 G conditions through a 310 nm thick ITO NC-coated glass at different electrical potentials. Potentials (positive bias) at which the LSPR contribution decreases are termed as 'bleached' state, and those (negative bias) at which LSPR increases are termed as 'coloured' state. Clearly, the NIR contribution of the solar spectrum is strongly modulated by electric field, while transmittance of visible light is similar for both the bleached and coloured state. Bleached state exhibits 35% more transmittance in the NIR region of solar spectrum than the coloured state. Therefore, ITO NC (or other suitable TCO NC) coated glass could be suitable for smart windows application, where bleached state increases the temperature of a highly glazed building via transmitting the NIR region of solar light, and coloured state can block the NIR light decreasing

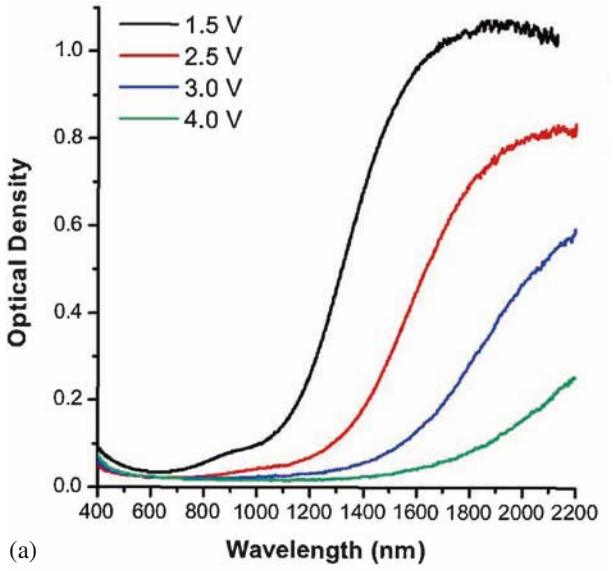

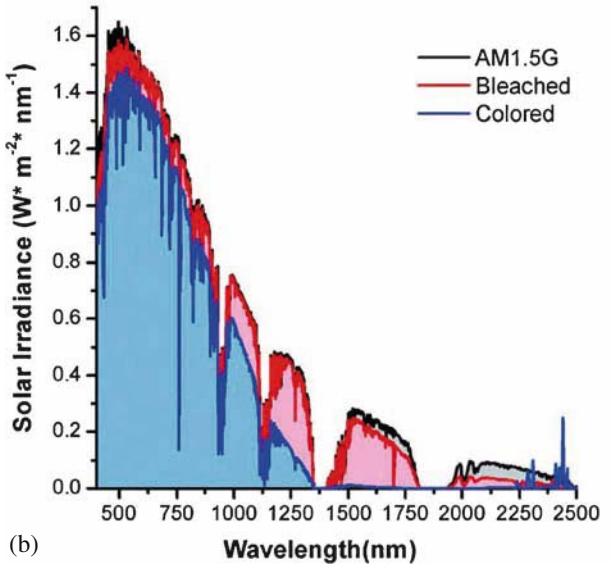

Figure 5. (**a**) Electrochemical modulation of LSPR spectra of a film made of 16.8% Sn-doped In_2O_3 NCs (4.1 nm diameter) on applying different bias voltage. (**b**) Transmittance of bleached (positively biased) and coloured (negatively biased) states of 310 nm thick film of 16.8% Sn-doped In_2O_3 NCs film in AM 1.5G solar spectrum range (reprinted with permission from ref. [38]).

the temperature inside the building. Importantly, both coloured and the bleached states have similar visible light transmittance. This modulation of NIR light transmittance using an electric field, without affecting the visible light transmittance is a key feature of TCO NCs.

4.2 *Magnetic and plasmonic Sn–Fe-codoped In_2O_3 for photothermal therapy*

Combination of NIR LSPR and strong magnetic response in solution-processed NCs is needed for photothermal therapy-based treatment of selective tumour cells. Magnetic response provides contrast in magnetic resonance imaging (MRI) to identify and locate the diseased cell. Absorption of NIR light by the same NC attached to the diseased cell generates heat, destroying the cell. Nanocomposites or core/shell NCs, for example, Fe_3O_4/Au [42,43] and $Fe_3O_4/Cu_{2-x}S$ [44] NCs have been attempted where the core exhibits ferromagnetism and shell exhibits NIR LSPR. Heterostructured NCs, where a metallic component is responsible for LSPR, for example in Fe_3O_4/Au core/shell NCs, do not easily exhibit LSPR in NIR region. A large dimension, typically larger than 50 nm, is required for Au NCs to exhibit NIR (>1000 nm) LSPR. Such large NCs are not desirable for *in vivo* applications. Recently, we reported the coexistence of weak ferromagnetism at room temperature and NIR LSPR in Fe–Sn-codoped In_2O_3 NCs with an average diameter of 6.5 nm [10]. Such NCs would be suitable for localized photothermal therapy.

5. Conclusions

TCO NCs have already been established as novel plasmonic materials. The LSPR from TCO NCs are intrinsically different from that of a metal NC, suggesting the possibilities of new kinds of applications of LSPR obtained from TCO NCs. The origin of LSPR in TCO NCs, such as Sn-doped In_2O_3 NCs, is related to the free electron generated by the dopant (Sn^{4+}) in the conduction band of the host (In_2O_3) NCs, and can be explained by modified Drude model. Doped NCs such as Sn-doped In_2O_3, Al, Ga or In-doped ZnO, In-doped CdO and In–F codoped CdO NCs exhibit LSPR in their equilibrium steady-state population, where free electrons arise from doping. On the other hand, LSPR can also be obtained from undoped ZnO NCs upon photoexcitation, where the free electron generates after the absorption of UV radiation (energy higher than the bandgap) followed by scavenging the hole. The NIR LSPR from TCO NCs can be useful for dynamic smart windows for energy-efficient heating/cooling of a highly glazed building, and also for local treatment of a diseased cell using photothermal therapy.

Acknowledgements

AN acknowledges Science and Engineering Research Board (SERB) Govt. of India for the Ramanujan Fellowship (SR/S2/RJN-61/2012).

References

[1] G Frank and H Kostlin, *Appl. Phys. A-Mater. Sci. Process.* **27**, 197 (1982)
[2] A Nag and A Shireen, *Solid-State Commun.* **150**, 1679 (2010)
[3] Transparent Conductive Coatings: Technologies and Global Markets, 2014
[4] U Kreibig and M Vollmer, *Optical properties of metal clusters* (Springer, Berlin, 1995) Vol. 25
[5] M A El-Sayed, *Acc. Chem. Res.* **34**, 257 (2001)
[6] P Pramod and K G Thomas, *Adv. Mater.* **20**, 4300 (2008)
[7] R A Gilstrap, C J Capozzi, C G Carson, R A Gerhardt and C J Summers, *Adv. Mater.* **20**, 4163 (2008)

[8] Y X Zhao, H C Pan, Y B Lou, X F Qiu, J J Zhu and C Burda, *J. Am. Chem. Soc.* **131**, 4253 (2009)
[9] T Wang and P V Radovanovic, *J. Phys. Chem. C* **115**, 406 (2011)
[10] B Tandon, G S Shanker and A Nag, *J. Phys. Chem. Lett.* **5**, 2306 (2014)
[11] G S Shanker, B Tandon, T Shibata, S Chattopadhyay and A Nag, *Chem. Mater.* **27**, 892 (2015)
[12] G V Naik, V M Shalaev and A Boltasseva, *Adv. Mater.* **25**, 3264 (2013)
[13] J A Faucheaux, A L D Stanton and P K Jain, *J. Phys. Chem. Lett.* **5**, 976 (2014)
[14] S D Lounis, E L Runnerstrorm, A Llordes and D J Milliron, *J. Phys. Chem. Lett.* **5**, 1564 (2014)
[15] N Ashcroft and D Mermin, Solid state physics, Thomson Learning (1976)
[16] J Pérez-Juste, I Pastoriza-Santos, L M Liz-Marzán and P Mulvaney, *Coord. Chem. Rev.* **249**, 1870 (2005)
[17] M M Alvarez, J T Khoury, T G Schaaff, M N Shafigullin, I Vezmar and R L Whetten, *J. Phys. Chem. B* **101**, 3706 (1997)
[18] F Mark, *Optical properties of solids* (Oxford University Press, New York, 2001)
[19] J M Luther, P K Jain, T Ewers and A P Alivisatos, *Nat. Mater.* **10**, 361 (2011)
[20] A M Schimpf, N Thakkar, C E Gunthardt, D J Masiello and D R Gamelin, *ACS Nano* **8**, 1065 (2013)
[21] T Nütz, U Z Felde and M Haase, *J. Chem. Phys.* **110**, 12142 (1999)
[22] N M Torkaman, Y Ganjkhanlou, M Kazemzad, H H Dabaghi and M Keyanpour-Rad, *Mater. Character.* **61**, 362 (2010)
[23] S D Lounis, E L Runnerstrom, A Bergerud, D Nordlund and D J Milliron, *J. Am. Chem. Soc.* **136**, 7110 (2014)
[24] J H W de Wit, *J. Solid State Chem.* **20**, 143 (1977)
[25] J H W de Wit, *J. Solid State Chem.* **13**, 192 (1975)
[26] J H W de Wit, *J. Solid State Chem.* **8**, 142 (1973)
[27] J H W de Wit, G Van Unen and M Lahey, *J. Phys. Chem. Solids* **38**, 819 (1977)
[28] F A Kröger and H J Vink, Relations between the concentrations of imperfections in crystalline solids, in: *Solid state physics* edited by S Frederick, T David (Academic Press, 1956) pp. 307–435
[29] G Frank and H Köstlin, *Appl. Phys. A* **27**, 197 (1982)
[30] O Warschkow, D E Ellis, G B González and T O Mason, *J. Am. Cer. Soc.* **86**, 1707 (2003)
[31] T Minami, *Semicond. Sci. Technol.* **20**, S35 (2005)
[32] R Buonsanti, A Llordes, S Aloni, B A Helms and D J Milliron, *Nano Lett.* **11**, 4706 (2011)
[33] E D Gaspera, A S R Chesman, J van Embden and J J Jasieniak, *ACS Nano* **8**, 9154 (2014)
[34] T R Gordon, T Paik, D R Klein, G V Naik, H Caglayan, A Boltasseva and C B Murray, *Nano Lett.* **13**, 2857 (2013)
[35] X C Ye, J Y Fei, B T Diroll, T Paik and C B Murray, *J. Am. Chem. Soc.* **136**, 11680 (2014)
[36] J A Faucheaux and P K Jain, *J. Phys. Chem. Lett.* **4**, 3024 (2013)
[37] A M Schimpf, N Thakkar, C E Gunthardt, D J Masiello and D R Gamelin, *ACS Nano* **8**, 1065 (2014)
[38] G Garcia, R Buonsanti, E L Runnerstrom, R J Mendelsberg, A Llordes, A Anders, T J Richardson and D J Milliron, *Nano Lett.* **11**, 4415 (2011)
[39] K P Kadlag, M J Rao and A Nag, *J. Phys. Chem. Lett.* **4**, 1676 (2013)
[40] K P Kadlag, P Patil, M J Rao, S Datta and A Nag, *Crystengcomm.* **16**, 3605 (2014)
[41] R Baetens, B P Jelle and A Gustavsen, *Sol. Energy Mater. Sol. Cells* **94**, 87 (2010)
[42] R Bardhan, W X Chen, C Perez-Torres, M Bartels, R M Huschka, L L Zhao, E Morosan, R G Pautler, A Joshi and N J Halas, *Adv. Funct. Mater.* **19**, 3901 (2009)
[43] W J Dong, Y S Li, D C Niu, Z Ma, J L Gu, Y Chen, W R Zhao, X H Liu, C S Liu and J L Shi, *Adv. Mater.* **23**, 5392 (2011)
[44] Q W Tian, J Q Hu, Y H Zhu, R J Zou, Z G Chen, S P Yang, R W Li, Q Q Su, Y Han and X G Liu, *J. Am. Chem. Soc.* **135**, 8571 (2013)